Nonlinear properties of dispersion engineered InGaP photonic wire waveguides in the telecommunication wavelength range

Utsav D. Dave,[1, 2,*] Bart Kuyken,[1, 2] François Leo,[1, 2] Simon-Pierre Gorza,[3] Sylvain Combrie,[4] Alfredo De Rossi,[4] Fabrice Raineri,[5,6] and Gunther Roelkens[1, 2]

[1]Photonics Research Group, Department of Information Technology, Ghent University-IMEC, Ghent B-9000 Belgium

[2]Center for Nano- and Biophotonics (NB-photonics), Ghent University, Belgium

[3]OPERA-Photonique, Université Libre de Bruxelles (ULB), 50 Av. F. D. Roosevelt, CP 194/5, B-1050 Bruxelles, Belgium

[4]Thales Research and Technology, Route Départementale 128, 91767 Palaiseau, France

[5]Laboratoire de Photonique et de Nanostructures, CNRS-UPR20, Route de Nozay, 91460 Marcoussis, France

[6]Université Paris Denis Diderot, 75205 Paris, France

[*]utsav.dave@intec.ugent.be

Abstract: We propose high index contrast InGaP photonic wires as a platform for the integration of nonlinear optical functions in the telecom wavelength window. We characterize the linear and nonlinear properties of these waveguide structures. Waveguides with a linear loss of 12 dB/cm and which are coupled to a single mode fiber through gratings with a -7.5 dB coupling loss are realized. From four wave mixing experiments, we extract the real part of the nonlinear parameter γ to be 475±50 $W^{-1}m^{-1}$ and from nonlinear transmission measurements we infer the absence of two-photon absorption and measure a three-photon absorption coefficient of (2.5±0.5) x 10^{-2} cm^3GW^{-2}.

OCIS codes: (250.4390) Nonlinear optics, integrated optics; (190.4400) Nonlinear optics, materials; (190.3270) Nonlinear optics, Kerr effect; (190.4380) Nonlinear optics, four-wave mixing.

References and links

1. L.K. Oxenlowe, M. Pu, Y. Ding, H. Hu, F. Da Ros, D. Vukovic, A. Sellerup Jensen, H. Ji, M. Galili, C. Peucheret, and K. Yvind , "All-optical signal processing using silicon devices," European Conference on Optical Communication, ECOC'2014, Cannes, France, Sep. 2014.
2. E. Ryckeboer, A. Gassenq, M. Muneeb, N. Hattasan, S. Pathak, L. Cerutti, J.B. Rodriguez, E. Tournié, W. Bogaerts, R. Baets, and G. Roelkens, "Silicon-on-insulator spectrometers with integrated GaInAsSb photodiodes for wide-band spectroscopy from 1510 to 2300 nm," Opt. Express **21**(5), 6101 (2013).
3. F. Xia, L. Sekaric, and Y. Vlasov, "Ultracompact optical buffers on a silicon chip," Nat. Photonics **1**, 65 (2007).
4. N. Ophir, R. K. W. Lau, M. Menard, X. Zhu, K. Padmaraju, Y. Okawachi, R. Salem, M. Lipson, A. L. Gaeta, and K. Bergman, "Wavelength conversion and unicast of 10-Gb/s data spanning up to 700 nm using a silicon nanowaveguide," Opt. Express **20**(6), 6488 (2012).
5. A. Gajda, L. Zimmermann, M. Jazayerifar, G. Winzer, H. Tian, R. Elschner, T. Richter, C. Schubert, B. Tillack, and K. Petermann, "Highly efficient CW parametric conversion at 1550 nm in SOI waveguides by reverse biased p-i-n junction," Opt. Express **20**(12), 13100 (2012).
6. A. Liu, H. Rong, M. Paniccia, O. Cohen, and D. Hak, "Net optical gain in a low loss silicon-on-insulator waveguide by stimulated Raman scattering," Opt. Express **12**(18), 4261 (2004).
7. Q. Lin, O. J. Painter, and G. P. Agrawal, "Nonlinear optical phenomena in silicon waveguides: modeling and applications," Opt. Express **15**(25), 16604 (2007).

8. J. R. Ong, R. Kumar, and S. Mookherjea, "Silicon microring-based wavelength converter with integrated pump and signal suppression," Opt. Lett. **39**(15), 4439 (2014).
9. B. Kuyken, X. Liu, G. Roelkens, R. Baets, R. M. Osgood, and W. M. J. Green, "50 dB parametric on-chip gain in silicon photonic wires," Opt. Lett. **36**(22), 4401 (2011).
10. M. A. Foster, A. C. Turner, R. Salem, M. Lipson, and A. L. Gaeta, "Broad-band continuous-wave parametric wavelength conversion in silicon nanowaveguides," Opt. Express **15**(20), 12949 (2007).
11. G. Roelkens, L. Liu, D. Liang, R. Jones, A. Fang, B. Koch, and J. Bowers, "III-V/silicon photonics for on-chip and intra-chip optical interconnects," Laser and Photonics Reviews **4**(6), 751 (2010).
12. M. J. R. Heck, B. R. Koch, D. Liang, M. N. Sysak, and J. E. Bowers, "Hybrid silicon photonics for optical interconnects," IEEE J. Sel. Top. Quantum Electron. **17**(2), 333 (2011).
13. R. Halir, Y. Okawachi, J. S. Levy, M. A. Foster, M. Lipson, and A. L. Gaeta, "Ultrabroadband supercontinuum generation in a CMOS-compatible platform," Opt. Lett. **37**(10), 1685 (2012).
14. J. J. Wathen, P. Apiratikul, C. J. K. Richardson, G. A. Porkolab, G. M. Carter, and T. E. Murphy, "Efficient continuous-wave four-wave mixing in bandgap-engineered AlGaAs waveguides," Opt. Lett. **39**(11), 3161 (2014).
15. C. Husko, S. Combrie, Q. Vy Tran, F. Raineri, C. W. Wong, and A. De Rossi, ''Non-trivial scaling of self-phase modulation and three-photon absorption in III-V photonic crystal waveguides," Opt. Express **17**, 22442 (2009).
16. P. Colman, C. Husko, S. Combrié, I. Sagnes, C. W. Wong, and A. De Rossi, "Temporal solitons and pulse compression in photonic crystal waveguides," Nat. Photonics **4**, 862 (2010).
17. C. Lacava, V. Pusino, P. Minzioni, M. Sorel, and I. Cristiani, "Nonlinear properties of AlGaAs waveguides in continuous wave operation regime," Opt Express **22**(5), 5291 (2014).
18. C. Xiong, W. Pernice, K. K. Ryu, C. Schuck, K. Y. Fong, T. Palacios, and H. X. Tang, "Integrated GaN photonic circuits on silicon (100) for second harmonic generation," Opt. Express **19**(11), 10462 (2011).
19. M. Savanier, C. Ozanam, L. Lanco, X. Lafosse, A. Andronico, I. Favero, S. Ducci, and G. Leo, "Near-infrared optical parametric oscillator in a III-V semiconductor waveguide," App. Phys. Lett. **103**, 261105 (2013).
20. J. Aitchison, D. Hutchings, J. Kang, G. Stegeman, and A. Villeneuve, "The nonlinear optical properties of AlGaAs at the half bandgap," IEEE J. Quantum Electron. **33**, 341 (1997).
21. Q. Lin, T. J. Johnson, R. Perahia, C. P. Michael, and O. J. Painter, "A proposal for highly tunable optical parametric oscillation in silicon micro-resonators," Opt Express **16**(14), 10596 (2008).
22. V. Eckhouse, I. Cestier, G. Eisenstein, S. Combrié, P. Colman, A. De Rossi, M. Santagiustina, C. G. Someda, and G. Vadalà, "Highly efficient four wave mixing in GaInP photonic crystal waveguides," Opt. Lett. **35**(9), 1440 (2010).
23. M. Lamponi, S. Keyvaninia, C. Jany, F. Poingt, F. Lelarge, G. de Valicourt, G. Roelkens, D. Van Thourhout, S. Messaoudene, J.-M. Fedeli, and G. H. Duan, "Low-threshold heteroogeneously integrated InP/SOI laser with a double adiabatic taper coupler," IEEE Photon. Technol. Lett. **24**(1), 76 (2012).
24. J. Van Campenhout, P. Rojo-Romeo, P. Regreny, C. Seassal, D. Van Thourhout, S. Verstuyft, L. Di Cioccio, J.-M. Fedeli, C. Lagahe, and R. Baets "Electrically pumped InP-based microdisk lasers integrated with a nanophotonic silicon-on-insulator waveguide circuit," Opt Express **15**(11), 6744 (2007).

1. Introduction

Silicon-on-insulator (SOI) has become a very popular platform for various applications of integrated optics, especially in the field of telecommunications, but also in other fields like spectroscopy and sensing [1-12]. This is mainly related to the fact that low loss (~ 2 dB/cm) high index contrast waveguide structures can be realized on this platform using the CMOS processing infrastructure. Because the high index contrast allows large field intensities inside the waveguides, and since silicon also has a large third-order susceptibility (n_2 = 4x10^{-18} m^2/W), the SOI platform has been investigated for many nonlinear optics based applications [4-10]. Despite these advantages, silicon is not the ideal material for many nonlinear applications because it suffers from large nonlinear losses in the telecom wavelength region due to two-photon absorption and the resulting free-carrier absorption (TPA and FCA). This limits the efficiency of the nonlinear processes on silicon. Silicon also has no intrinsic second-order susceptibility due to its centrosymmetric crystal structure. III-V materials offer the possibility to overcome these disadvantages: they have a similarly high refractive index as

well as large second and third order nonlinearities. Some III-V material compositions such as InGaP or $Al_xGa_{1-x}As$ (both grown on a GaAs substrate) also have the advantage that the half-bandgap is larger than the photon energy in the telecommunications wavelength range and so should not suffer from TPA. This allows for efficient nonlinear optical processes in the telecommunication wavelength range. Heterogeneously integrated III-V materials on a silicon substrate have already been extensively studied for on-chip light generation [11-12, 23-24]. Previous studies have explored the nonlinear properties of photonic wire waveguides and photonic crystal waveguides realized on their III-V growth substrate based on different III-V materials, including InGaP, for a range of nonlinear optics applications [14-19, 22].

In this work we report the characterization of the nonlinear properties of InGaP high index contrast photonic wire waveguides integrated on a silicon substrate and separated from the substrate by a 3 μm thick thermal oxide layer. Many nonlinear processes are only efficient in the presence of phasematching, which can be achieved by engineering the waveguide dispersion profile. Waveguides with a high index contrast allow wide tuning of the dispersion by engineering the waveguide cross-section [13]. Hence, in order to fully exploit the large refractive index of III-V materials and achieve a high index contrast similar to the SOI platform, removal of the GaAs substrate used for the growth of the InGaP layer is necessary. Therefore we use the approach of bonding the InGaP layer, along with its growth substrate, to the silicon substrate after which the growth substrate is removed. The details of the fabrication of the InGaP waveguides on the silicon substrate and their linear properties are discussed in Section 2. In Section 3 we report the experiments performed to characterize the nonlinear properties of these waveguides. The nonlinear parameter γ is extracted from the measurement of the four wave mixing conversion efficiency. We also confirm the absence of two-photon absorption and measure the three-photon absorption coefficient through nonlinear transmission measurements.

2. Fabrication

For fabricating the InGaP photonic wire waveguides, a 250 nm thick InGaP layer is first grown lattice matched to a GaAs substrate. It is separated from the substrate by a 1.4 μm thick GaAs sacrificial layer and a 200 nm thick InGaP etch-stop layer. A 200 nm thick SiO_x layer is deposited on top of this III-V stack, after which the III-V stack is bonded upside-down onto the silicon substrate, which has a 3 μm thick thermal oxide buffer layer on top to isolate the optical mode from the silicon substrate. The bonding is done using a 35% Benzocyclobutene (BCB) solution spun at 1000 rpm, which results in a 1 μm thick BCB layer. Subsequently, the GaAs substrate is removed via wet etching in a nitric acid solution (HNO_3:H_2O_2:H_2O in a volume ratio of 1:4:1). The InGaP etch-stop layer is selectively removed using a 1:1 vol mixture of HCl and H_3PO_4, after which the GaAs sacrifical layer is again removed using the nitric acid solution. Fabrication of the strip waveguides in the InGaP membrane is done via e-beam lithography and inductively coupled plasma (ICP) etching using a HBr/O_2/He gas mixture (100:0.6:60 sccm) giving an etch rate of about 5 nm/sec. A two-step etching process is used to fabricate partially etched gratings in the InGaP layer to couple light into the waveguides. In the first step, the waveguides are written using the negative tone resist hydrogensilsesquioxane (HSQ) and etched in the ICP. In the second step, the gratings are written in the positive tone resist polymethylmethacrylate (PMMA), which is

used to etch a silicon nitride hard mask using reactive ion etching (RIE) prior to the final ICP etching step. The gratings have a period of 725 nm, a fill factor of 50%, and are etched 50 nm deep into the 250nm thick InGaP membrane. The fiber-to-chip coupling efficiency to a single mode fiber at a 10° coupling angle is shown in Fig. 1(c) and peaks at -7.6 dB at 1540nm wavelength (with a 3 dB bandwidth of 45 nm) for TE-polarized light.

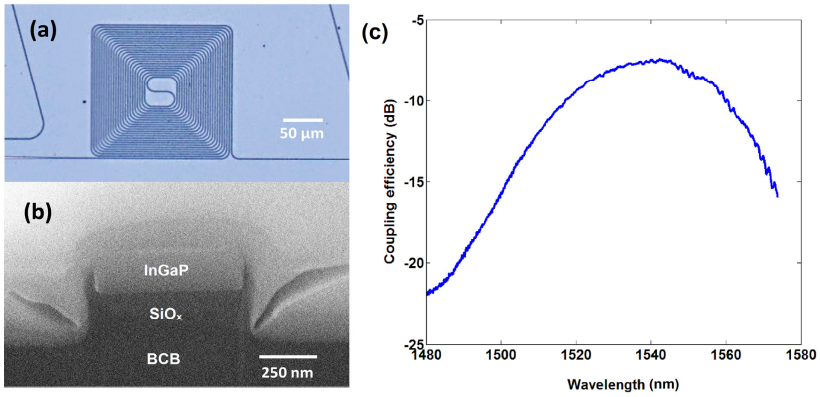

Fig. 1. (a) A 1 cm long InGaP waveguide with small footprint due to the high index contrast; (b) the SEM cross-section of the InGaP waveguide with measured dimensions of 630 nm x 250 nm; (c) the coupling efficiency of the shallow etched grating as a function of wavelength showing a maximum efficiency of -7.5 dB at 1540 nm (TE polarization).

Due to the high index contrast, it is possible to fit a 1 cm long waveguide in an area of just 180 µm x 180 µm, as shown in Fig. 1(a). The fabricated waveguides (cross-section 630 nm x 250 nm as measured using SEM, see Fig. 1(b)) have a linear loss of 12±0.5 dB/cm (TE polarization at 1540 nm) measured using a cutback method. The large linear losses are thought to originate from sidewall scattering and can be reduced by improving the etching of the waveguides.

As stated above, due to the high index contrast of these waveguides dispersion engineering is easily achievable by changing the waveguide dimensions. For example, the dispersion of the fundamental TE-like mode at 1550 nm wavelength is tuned from the normal to the anomalous regime simply by changing the width of the waveguide as shown in Fig. 2 where the simulated dispersion of various waveguides with different widths and a fixed height of 250 nm are presented. Of course, dispersion could also be tuned by changing the height of these waveguides, which can be done at the growth stage prior to bonding. It can be seen that for waveguides with widths between 500-700 nm, it is possible to have anomalous dispersion in the telecom wavelength range, which is critical for numerous nonlinear applications.

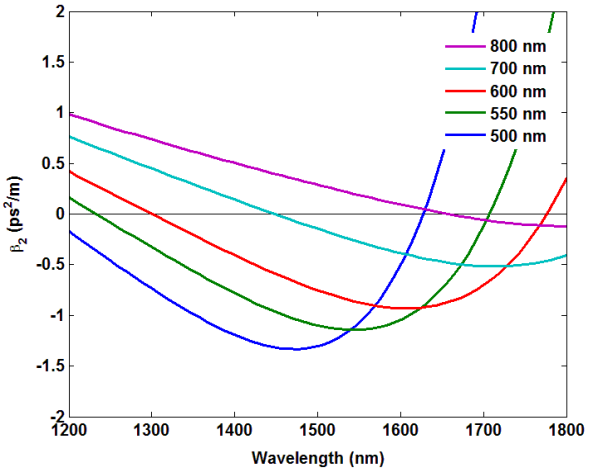

Fig. 2. The simulated dispersion for waveguides of height 250 nm and widths ranging from 500 to 800 nm shows that dispersion engineering in this high index contrast platform allows access to the anomalous dispersion regime.

3. Characterization of the nonlinear properties of the InGaP photonic wires

The third order nonlinearity is characterized by the nonlinear parameter γ defined as:

$$\gamma = \frac{k_0 n_2}{A_{eff}} + i\frac{\beta_{TPA}}{2A_{eff}} \tag{1}$$

Here, n_2 is the nonlinear Kerr index and A_{eff} is the effective area of the waveguide for third-order processes defined as $\left(\iint |E|^2\, dxdy\right)^2 \Big/ \iint |E|^4\, dxdy$ [20], which for our waveguide is calculated to be 0.24 μm^2. Obviously, if there is no TPA, then the imaginary part of γ is zero. In the case of InGaP lattice matched to GaAs, the bandgap is 1.9 eV, which is larger than twice the photon energy at 1550 nm wavelength (0.8 eV); hence we expect no two-photon absorption. In that case, the dominant multi-photon loss mechanism would be the three-photon absorption (3PA). Of course, the carriers generated through such a nonlinear absorption process also cause extra losses through FCA.

3.1 Nonlinear loss

In order to confirm that the material indeed does not suffer from TPA, we measure the transmission T of a pulsed laser (producing hyperbolic secant pulses with a FWHM of 2.8 ps measured with an intensity autocorrelator) through a 1 cm long InGaP waveguide. The measured output peak power vs the input peak power is shown in Fig. 3. It can be seen that due to nonlinear losses the output power does not increase linearly with the input power. If these nonlinear losses occur due to TPA, then the reciprocal of the transmission should increase linearly with the input peak power. However, as shown in Fig. 4(a), we observe that that's not the case for the InGaP waveguide. The $1/T^2$ trend however is linear with respect to the square of the input peak power as shown in Fig. 4(b) which points towards three-photon

absorption being the dominant multi-photon loss mechanism in these InGaP photonic wires [14, 15]. The equation governing the transmission through a 3PA dominated waveguide is $dI/dz = -\alpha I(z) - \alpha_3 I(z)^3$ where I is the intensity at position z along the waveguide, α is the linear absorption term and α_3 is the bulk 3PA coefficient. Equation (2) below describes the transmission of a $sech^2$ pulse as a function of the input intensity [14]:

$$T = \int_{-\infty}^{\infty} \frac{\frac{1}{2t_0} e^{-\alpha L} \operatorname{sech}^2\left(\frac{t}{t_0}\right)}{\left[1 + \frac{\alpha_3}{\alpha} I_0^2 \operatorname{sech}^4\left(\frac{t}{t_0}\right)\left(1 - e^{-2\alpha L}\right)\right]^{\frac{1}{2}}} dt \qquad (2)$$

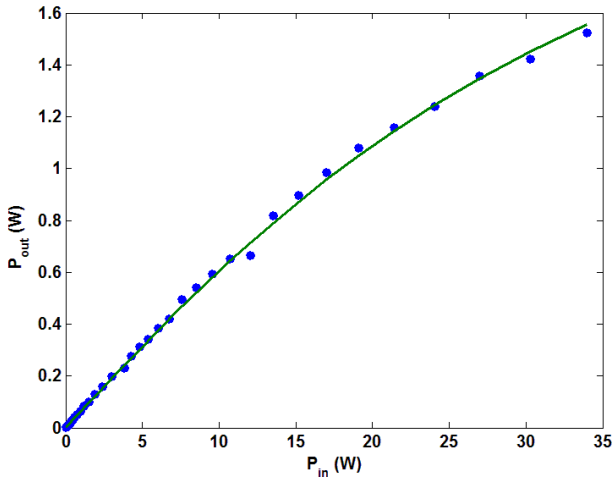

Fig. 3. The measured output peak power as a function of the input peak power (circles) and the best-fit using Eq. (2) which gives a α_3 value of 2.5×10^{-2} cm^3/GW^2.

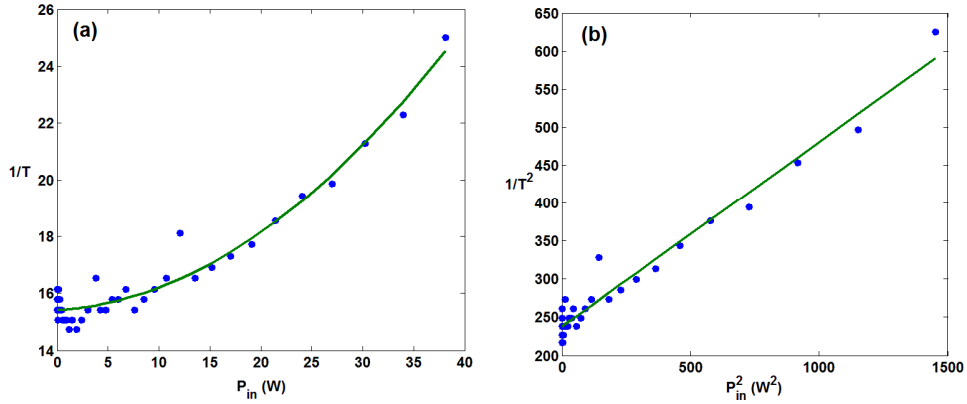

Fig. 4. (a) The reciprocal transmission is not a linear function of input peak power while, (b) the reciprocal transmission squared increases linearly with the input peak power squared clearly showing that there is no two-photon absorption in these waveguides due to the large bandgap of InGaP.

Here, L is the length of the waveguide and I_0 is the input intensity at the peak of the pulse. Using Eq. (2) with the 3PA coefficient as the unknown parameter, we fit experimental data of the output power as a function of the input peak power (Fig. 3, solid line). We extract the α_3

value to be (2.5±0.5) x10^{-2} cm^3/ GW^2 which is close to other reports in literature [16]. Clearly, the InGaP waveguides do not suffer from two-photon absorption in the telecommunication wavelength range, as expected from its bandgap value.

3.2 Measurement of the nonlinear parameter γ

For characterizing the nonlinear parameter γ, a four-wave mixing experiment was carried out in the low power continuous wave regime where the probe signal is close to the pump wavelength (Δλ<1 nm), in order for the phase mismatch ($|\Delta k|L = \Delta\omega^2|\beta_2|L \approx 10^{-3}$) to be negligible and the conversion efficiency maximal. In this regime, the conversion efficiency, defined as the ratio of the idler output power to the signal output power, has a quadratic dependence on the nonlinear parameter [17]:

$$\eta = \frac{P_{idl}(\mathrm{L})}{P_{sig}(\mathrm{L})} = \left(\gamma P_{pump}(0) L_{eff}\right)^2 \qquad (3)$$

Here, L_{eff} defined as $(1-e^{-\alpha L})/\alpha$ is the effective interaction length taking into account the propagation loss α along the waveguide. For the waveguide used in this experiment (2 mm length) this results in an effective interaction length of 1.54 mm. Figure 5(a) shows the output spectrum of the pump, signal and idler wavelengths showing a conversion efficiency of -31 dB for coupled pump and probe input powers of 38 mW and 1.47 mW respectively.

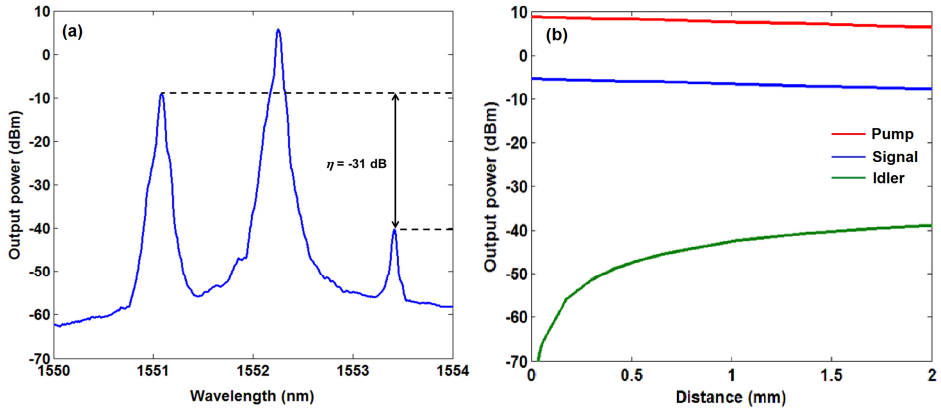

Fig. 5. (a) The measured output spectrum of the pump, signal and idler showing a conversion efficiency of -31 dB and (b) the simulated evolution of the pump, signal and idler power (taking into account -7.5 dB outcoupling efficiency) along the waveguide for γ = 475 $W^{-1}m^{-1}$.

In order to confirm the validity of Eq. (3) in this regime and extract the nonlinear parameter γ, we did numerical simulations of the following coupled wave equations for degenerate four-wave mixing [21]:

$$\frac{dA_s}{dz} = i\gamma\frac{\omega_s}{\omega_p}\left[\left(|A_s|^2 + 2|A_i|^2 + 2|A_p|^2\right)A_s + A_i^* A_p A_p e^{i\Delta kz}\right] - \frac{\alpha_{lin}}{2}A_s \qquad (4)$$

$$\frac{dA_i}{dz} = i\gamma \frac{\omega_i}{\omega_p}\left[\left(\left|A_i\right|^2 + 2\left|A_s\right|^2 + 2\left|A_p\right|^2\right)A_i + A_s^* A_p A_p e^{i\Delta kz}\right] - \frac{\alpha_{lin}}{2}A_i \quad (5)$$

$$\frac{dA_p}{dz} = i\gamma\left[\left(\left|A_p\right|^2 + 2\left|A_i\right|^2 + 2\left|A_s\right|^2\right)A_p + 2A_p^* A_s A_i e^{-i\Delta kz}\right] - \frac{\alpha_{lin}}{2}A_p \quad (6)$$

Here, $A_{s,i,p}$ represents the complex electric field amplitude of the signal, idler and pump waves respectively, z is the position along the waveguide, Δk is the phase mismatch and α_{lin} is the linear propagation loss in m^{-1}. Since we are working in the low power continuous wave regime, the nonlinear loss terms are negligible. Figure 5(b) shows the evolution of the pump, signal and idler power as a function of the length of the waveguide for the experimental conditions of Fig. 5(a) assuming a nonlinear parameter γ of 475 $W^{-1}m^{-1}$ and taking into account the -7.5 dB fiber coupling efficiency. Comparing that to Fig. 5(a), we see that the simulation gives the measured output power for the generated idler wave. We further measured the conversion efficiency as a function of the pump power. Fig. 6 shows the experimental data (circles) and the theoretical as well as the numerically simulated efficiency for γ = 475 $W^{-1}m^{-1}$. As can be seen, they agree very well, confirming the validity of Eq. (3). Thus we extract a value of the nonlinear parameter as 475±50 $W^{-1}m^{-1}$ with the uncertainty coming from the uncertainty on the waveguide coupled power.

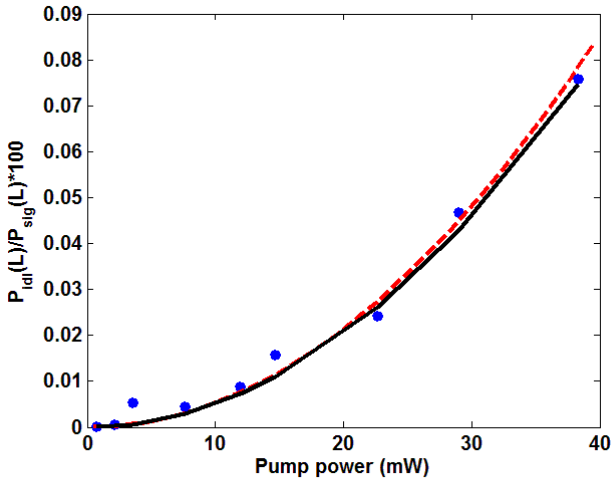

Fig. 6. The measured conversion efficiency (circles) as a function of the pump power and the theoretical (dashed line) and simulated (solid line) fits for γ = 475 $W^{-1}m^{-1}$.

4. Conclusions and outlook

We have demonstrated a new platform for on-chip nonlinear optics based on InGaP-on-insulator photonic wire waveguides. It benefits from the high-index contrast of the waveguides – which enables both dispersion engineering and large optical intensities – and a large third-order nonlinearity characterized by a nonlinear parameter γ of 475 $W^{-1}m^{-1}$ as well as no two-photon absorption in the telecommunications wavelength range. A nonlinear

parameter γ of 521 $W^{-1}m^{-1}$ and 2900 $W^{-1}m^{-1}$ has previously been reported in other approaches employing different III-V materials (AlGaAs waveguides [17]) or using free standing slow light InGaP photonic crystal waveguides [22] respectively. The γ value obtained here could be further optimized by engineering the waveguide cross section or employing other III-V materials with higher n_2 values such as AlGaAs using a similar procedure to the one used here. The advantage of our approach of bonding the III-V layer to a silicon substrate is that the nonlinear InGaP waveguide can be optically coupled to a SOI or SiN-on-insulator optical waveguide circuit, enabling easy integration with other well-developed linear devices on such platforms. Techniques developed for heterogeneously integrating III-V lasers on the SOI platform can be employed here. For example, adiabatic tapers in both the silicon and III-V layers can be used to couple light between the SOI and the III-V waveguide layer [23]. Microdisk resonators in the III-V layer can also be coupled to an underlying silicon waveguide [24]. Thus, it is a promising approach for a variety of applications in particular for all-optical signal processing in telecommunications. The use of III-V materials also creates the possibility to exploit their inherently large second-order nonlinearity. These avenues will be explored in future work.

Acknowledgments

The current work is supported by the FP7-ERC-MIRACLE project and by the Belgian Science Policy Office (BELSPO) Interuniversity Attraction Pole (IAP) project Photonics@be.